NIH Public Access
Author Manuscript
J Pharm Pharmacol. Author manuscript; available in PMC 2009 September 27.

Published in final edited form as:
J Pharm Pharmacol. 2008 August ; 60(8): 1049–1060. doi:10.1211/jpp.60.8.0011.

Assessment of Tissue Redox Status Using Metabolic Responsive Contrast Agents and Magnetic Resonance Imaging

Fuminori Hyodo, **Benjamin P. Soule**, **Ken-ichiro Matsumoto**, **Shingo Matusmoto**, **John A. Cook**, **Emi Hyodo**, **Anastasia L. Sowers**, **Murali C. Krishna**, and **James B. Mitchell***
Radiation Biology Branch, Center for Cancer Research, National Cancer Institute, NIH, Bethesda, MD, USA

Abstract

Regulation of tissue redox status is important to maintain normal physiological conditions in the living body. Disruption of redox homeostasis may lead to oxidative stress and can induce many pathological conditions such as cancer, neurological disorders, and aging. Therefore, imaging of tissue redox status could have clinical applications.

Redox imaging employing magnetic resonance imaging (MRI) with nitroxides as cell permeable redox sensitive contrast agents has been used for non-invasive monitoring of tissue redox status in animal models. The redox imaging applications of nitroxide EPRI and MRI are reviewed here, with a focus on application of tumor redox status monitoring. While particular emphasis has been placed on differences in the redox status in tumors compared selected normal tissues, the technique possesses the potential to have broad applications to the study of other disease states, inflammatory processes, and other circumstances where oxidative stress is implicated.

Keywords

redox status; EPRI; MRI; nitroxide; non-invasive imaging; free radical; Tempol

Introduction

In vivo molecular imaging research is an emerging discipline in medical research (Margolis et al 2007) and there has been considerable progress in the development of especially in small animal imaging research (Koo et al 2006). Computed Tomography (CT), Position Emission Tomography (PET), Single Photon Emission Computed Tomography (SPECT), Magnetic Resonance Imaging (MRI), and optical imaging are being used to visualize patho/pysiological conditions non-invasively (Herholz et al 2007; Torigian et al 2007). One of the prevalently used molecular imaging techniques is 18-fluorodeoxyglucose (FDG) with PET technique (Hoh 2007). MRI and PET have allowed clinicians to correlate anatomic abnormalities with biochemical attributes to better identify metastatic lesions. Such non-invasive imaging techniques can provide better and more patient-specific treatment since therapy can be tailored to the disease specifically (Huzjan et al 2005; Herholz et al 2007; Hoh 2007).

The redox environment (Schafer & Buettner 2001) within the tumor cell is an important parameter that may determine the response of a tumor to certain chemotherapeutic agents, radiation, and bio-reductive hypoxic cell cytotoxins (Mitchell & Russo 1987; Yu & Brown

*Correspondence to: Building 10, Room B3B69, NIH, Bethesda, MD 20892-1002. Tel: 301-496-7511. Fax: 301-480-2238. jbm@helix.nih.gov.

NIH-PA Author Manuscript
NIH-PA Author Manuscript
NIH-PA Author Manuscript

NIH-PA Author Manuscript

NIH-PA Author Manuscript

NIH-PA Author Manuscript

1984; Stratford et al 1994). A variety of intracellular molecules may contribute to the overall redox status in tissues including GSH, 3 thioredoxins, NADPH, flavins, ascorbate, and others (Schafer & Buettner 2001). Collectively, the reducing species may have an impact on how a particular tissue responds to oxidative stress induced by a particular drug or treatment modality, and, therefore, a non-invasive means of determining the redox status of a tissue should be a useful adjunct for clinical oncology. In addition, breakdown of redox balance may lead to oxidative stress and can induce many pathological conditions such as cancer, neurological disorders, and aging (Halliwell & Gutteridge 1999). Therefore, imaging of tissue redox status and monitoring the antioxidant level could be useful potentially in the diagnosis of disease states and in the assessment of treatment response in the case of cancer. Electron Paramagnetic Resonance Imaging (EPRI) is an imaging modality, which detects unpaired electrons in such species as transition metal complexes and free radicals and using magnetic field gradients, provides spatial distribution of free radicals (Kuppusamy et al 1994; Subramanian et al 2004) (Kuppusamy et al 1994; Liu et al 1995). Free radicals are present at extremely low levels in tissue, below the detection limits of EPR. Whereas this was initially felt to be a limitation to the use of this technique in biological imaging, it was quickly discovered that agents containing unpaired electrons, or agents converted to such a compound in vivo, could be introduced into a living system and detected using frequencies similar to those used in magnetic resonance imaging (MRI). This review focuses on the application of redox imaging for tumor redox status using EPRI or MRI and redox sensitive contrast agents.

Nitroxides as Antioxidants and Redox Probes

Stable nitroxide free radicals and their one-electron reduced products, namely the hydroxylamines are recycling antioxidants (Soule et al 2007). By undergoing one-electron transfer reactions, nitroxides are reduced to the corresponding hydroxylamines or oxidized to the corresponding oxoammonium cation species (Figure 1). Therefore, nitroxides are redox-active species, which can be oxidized or reduced by the corresponding reactants in cells and tissues. Once administered in vivo, all three forms can exist. Nitroxides can undergo oxidation to the corresponding oxoammonium cation by various oxidants such as hypervalent heme, $HO_2\cdot$, $CO_3^{-}\cdot$, and $NO_2^{-}\cdot$ radicals (Krishna et al 1992; Krishna et al 1996a; Krishna et al 1996b; Goldstein et al 2006). Thus, in tumors, low levels of oxidative stress may generate these species, which can decrease the nitroxide levels faster than in normal tissue. Oxoammonium cations can be reduced to the nitroxide state by superoxide at diffusion-limited rates or to the hydroxylamine by 2-electron reducing agents(Krishna et al 1996a). Nitroxides can also be reduced to the corresponding hydroxylamines by reductants such as ascorbate, semiquinone radical, and also by intercepting reducing equivalents from the electron transport chain(Swartz 1990). The hydroxylamines can be oxidized to the nitroxides in the presence of hydrogen peroxide and other oxidants such as transition metal complexes(DeGraff et al 1994). In vitro, nitroxides were found to undergo accelerated conversion to hydroxylamines under hypoxic conditions compared with normoxia (Chen et al 1989). Furthermore, in normoxic cells, the conversion was significantly retarded when the thiol levels were depleted or in cells deficient in the enzyme glucose-6- phosphate dehydrogenase(Kuppusamy et al 2002; Samuni et al 2004). The nitroxide/oxoammonium cation pair constitutes an efficient redox couple and mimics the enzymic action of superoxide dismutase (SOD) in a pH dependent manner(Krishna et al 1996a) and also confers catalase-like action to heme proteins such as myoglobin, cytochrome C etc.(Krishna et al 1996b). The nitroxide radical, though chemically stable, can participate in radical-radical recombination reactions with a variety of free radicals possessing a wide range of reactivities. The hydroxylamine on the other hand, can function as a classic antioxidant such as thiols, ascorbate, etc. by donating the H-atom. Its reaction efficiencies depend on the species with which it interacts. With highly reactive species such as OH radicals, the hydroxylamine is an efficient scavenger; whereas, with species of moderate oxidation potential, hydrogen atom donation by the hydroxylamine proceeds slowly.

NIH-PA Author Manuscript

NIH-PA Author Manuscript

NIH-PA Author Manuscript

As mentioned above, nitroxides exert SOD-mimic activity. SOD is an antioxidant enzyme that detoxifies superoxide ($O_2 \cdot^-$) but is too large to cross cell membranes making it difficult to accumulate intracellularly by adding exogenous SOD. Unlike SOD, nitroxides can readily cross cell membranes and thus provide intracellular antioxidant availability (Mitchell et al 2000) Nitroxides have been shown to protect against superoxide, hydrogen peroxide, organic peroxides and ionizing radiation (Mitchell et al 2000).

Nitroxides as EPRI Contrast Agents

Nitroxides have been used as in vivo EPR spectroscopy/imaging probes to elucidate redox mechanisms in many disease models (Berliner et al 1987; Kuppusamy et al 1998; Kuppusamy et al 2002; Yamada et al 2002; Utsumi & Yamada 2003). Nitroxides were found in vivo to be in an equilibrium between the nitroxide radical form which is detected by EPR, and the reduced form, the hydroxylamine, which is not detected by EPR because of its diamagnetic nature (Samuni et al 1990; Swartz 1990). This equilibrium is dependent on the surrounding environment, specifically tissue oxygen and the levels of reducing equivalents of the tissue milieu(Swartz 1990). Cellular redox processes convert the compound between the two states, thus the ratio of the two states is determined by the redox status within the cell (Figure 1B). Since only the oxidized form of the nitroxide can be detected using EPR, signal intensity can be used as a surrogate marker for the relative amounts of the oxidized compound and, therefore, the relative redox activity. In hypoxic cells (which are present in many tumors), the hydroxylamine form is more prevalent; whereas, the compound can be oxidized to the radical form in well oxygenated tissues (Swartz et al 1986b). This property of nitroxides makes them ideal compounds for studying intracellular redox metabolism.

The redox environment (Schafer & Buettner 2001) of the tumor is an important parameter that may determine the response of a tumor to certain chemotherapeutic agents, radiation, and bio-reductive hypoxic cell cytotoxins (Griffith 1982; Yu & Brown 1984; Mitchell & Russo 1987; Brown 1993; Stratford et al 1994). A variety of intracellular molecules may contribute to the overall redox status in tissues including glutathione (GSH), thioredoxins, NADPH, flavins, ascorbate, and others (Schafer & Buettner 2001). Collectively, the reducing species may have an impact on how a particular tissue responds to oxidative stress induced by a particular drug or treatment modality. Therefore, a non-invasive means of determining the redox status of a tissue should be a useful adjunct in clinical oncology.

The bioreduction of nitroxides in RIF-1 tumors implanted in mice was compared to that in normal tissue (Kuppusamy et al 2002; Yamada et al 2002). Pharmacokinetics of nitroxide uptake and clearance from normal and tumor tissues of RIF-1 tumor-bearing mice were measured *in vivo* using EPR spectroscopy (Figure 2 and 3A). EPR spectra were measured continuously from the tumor on right leg or normal muscle tissue on the left leg following injection of the nitroxide carbamoyl-PROXYL (3-carbamoyl-2,2,5,5-tetramethylpyrrolidine-N-oxyl, 3CP). Using this technology, two-dimensional images of the tumor revealed significant heterogeneity in both nitroxide distribution and rate of reduction (Figure 3B and C). Nitroxide concentrations in the tumor as well as normal tissues decreased linearly with time, suggesting that the clearance pharmacokinetics could be modeled by a pseudo-first order rate equation. Disappearance of the nitroxide was faster in tumor compared to normal muscle tissue (Kuppusamy et al 1998). A series of studies were conducted to determine if the reduction profiles in tumors could be altered by oxygenating the tumor by allowing the tumor-bearing animal to breathe carbogen. Upon oxygenating the tumor, EPRI was conducted as described above and significantly slower nitroxide reduction rates in the tumor were observed (Kuppusamy et al 1998). These data were consistent with the notion that cell/tissue hypoxia is an effective means to reduce nitroxides. The influence of endogenous thiols such as GSH, which is important in maintaining the intracellular redox balance, was also evaluated by using

NIH-PA Author Manuscript

NIH-PA Author Manuscript

NIH-PA Author Manuscript

inhibitors of GSH synthesis or agents that bind and deplete GSH (Kuppusamy et al 2002; Yamada et al 2002). When GSH levels were depleted in the tumor by 40–50%, EPRI assessed nitroxide reduction rates in the tumor were markedly slower. Collectively, the EPRI nitroxide reduction studies established: (*a*) the nitroxide is reduced more rapidly in the tumor tissue compared with normal muscle tissue in the tumor-bearing mice; (*b*) the nitroxide reduction rate constant is decreased when GSH levels are partially depleted or when the tumor oxygen concentration was increased by carbogen breathing. While the EPRI studies were important in establishing "proof of principle" for redox imaging, the lack of anatomic information from the EPRI and the long imaging times required for 3D imaging precluded its further development.

Nitroxides as MRI Redox Active Contrast Agents

As mentioned above, EPRI lacks the ability to co-register anatomy with the images of nitroxides' spatial distribution (Kuppusamy et al 1998; Kuppusamy et al 2002; Hyodo et al 2008; Matsumoto et al 2006; Cotrim et al 2007). MRI provides images with useful spatial and temporal resolutions and, with the use of suitable contrast agents, can provide important functional information pertaining to blood flow, and tissue perfusion. A number of applications with regard to characterization of disease and assessment of disease response to therapy have emerged using well established techniques in MRI and suitable choice of contrast media (Silva et al 2000; Barbier et al 2001; Dunn et al 2002; Shapiro et al 2004; Provenzale et al 2006). Conventional contrast agents used for T_1-contrast enhancement in MRI contain paramagnetic entities such as Gd^{3+} and Mn^{2+} complexes. Nitroxide radicals have a single unpaired electron and can provide T_1-contrast similar to gadolinium complexes. Although nitroxides (0.16 ~ 0.18 $mM^{-1}\ s^{-1}$) compare unfavorably to Gd^{3+}-containing agents in terms of relaxivity (3.7 $mM^{-1}{\cdot}sec^{-1}$), they are cell permeable and have a larger volume of distribution meaning they can provide useful T_1-contrast enhancement per unit volume (Hyodo et al. 2008).

The feasibility of using nitroxides as T_1-contrast agents was examined in the early days of MRI contrast probe development (Brasch 1983; Brasch et al 1983) and prior to their use as in vivo EPRI probes (Berliner & Fujii 1985). However, at the time they were found not to be optimal MRI contrast agents (Keana & Pou 1985) because in vivo, the paramagnetic nitroxide radicals were reduced to the undetectable diamagnetic hydroxylamine they were thus deemed "unstable" contrast probes for MRI (Swartz et al 1986a; Keana et al 1987; Chen et al 1989). Because of our experience with nitroxides in EPRI as described above and with the time-efficient image data acquisition strategies standard in current MRI scanners, we reevaluated nitroxides as *functional* redox sensitive probes using MRI. There are many technical challenges using nitroxide contrast agents in MRI. Nitroxide relaxivity is 20 times less than Gd^{3+} complexes. Additionally since nitroxides can react with reducing species in the body, they easily loose contrast ability. Therefore fast acquisition sequences and high field magnets are required. The major advantages of using nitroxides in MRI as opposed to EPRI include the availability of high resolution MRI scanners for both human and small animal studies, multi-slice imaging capability, enhanced spatial and temporal resolution, and co-registration of images of tissue redox status with anatomical/functional (water apparent diffusion coefficient, blood flow, blood volume etc.) information which can be available from MRI. The image enhancement in MRI is dependent on the original T_1 relaxation time of the tissue examined and its variation by free radicals, which is related to the accessibility of the radical to water protons. Therefore, image enhancement in tissue with a given T_1 should depend on the nitroxide concentration (Figure 4). On the other hand, image enhancement is affected by change of spectral shape and height in EPRI in addition to the concentration (Figure 4) (Matsumoto et al 2007). The near-independence of the relaxivity on the nature of nitroxide makes it easy to compare tissue redox status by MRI, whereas in EPRI, the line width and spectral multiplicity determines the image quality in terms of resolution and dynamic range. Continuous measurements of nitroxide levels shown detect similar decay rates from all three modalities

NIH-PA Author Manuscript

NIH-PA Author Manuscript

NIH-PA Author Manuscript

(Figure. 5). The similar decay rates obtained from the phantom using MRI and EPRI, which is an accepted method in monitoring nitroxide levels validate the use of MRI for such studies. Multi-slice images were obtained in 20 s using SPGR method (Figure 5C). This scanning allows fast pharmacokinetic imaging, besides providing detailed anatomical structure unlike in EPRI. In addition to anatomical structure, dynamic information such as blood flow, blood volume and water diffusion coefficients, etc., can be monitored by MRI and compared with redox images.

In Vivo Redox MRI of Tumor Redox Status

Nitroxide reduction as assessed by MRI or EPRI was first validated in phantoms containing the nitroxide with a reducing agent (Matsumoto et al 2006). Both EPRI and MRI experiments showed similar nitroxide reduction rates, suggesting that the T1 contrast capability of nitroxides was amenable to monitoring changes in image intensity using MRI. Next, differences in nitroxide 3CP metabolism in tumor and normal tissues were evaluated in tumor-bearing mice as shown in Figure 6A. As can be seen in Figure 6B, the MRI signal intensity increased in both normal leg and tumor bearing leg following 3CP administration and reached a maximum. However, the subsequent decrease in signal intensity in the tumor region was faster than that seen in normal tissue (Figure 6B). The signal reduction rate in the regions of interest (ROI) chosen in the normal leg was observed to be approximately 60% that of the reduction rate in the ROI in tumor (Figure 6C). The rate of change of intensity in each pixel was computed and a parametric image showed that overall tumor reduction was elevated as compared to normal tissue (Figure 6D). The significant enhancement in image intensity induced by 3CP administration and the superior temporal and spatial resolution of MRI suggest that it is advantageous to monitor the pharmacokinetic distribution of nitroxides using T_1-weighted MRI instead of EPRI.

To confirm that the decrease in nitroxide image intensity as shown in Figures 6B-D was due to reduction instead of clearance an independent study was conducted (Hyodo et al 2006). Three different nitroxides were use of which two were cell permeable nitroxides (Tempol, 3CP) and one cell-impermeable nitroxide (3-carboxy-2,2,5,5,5-tetramethylpyrrolidine-l-oxyl (CxP)). Reduction of these nitroxides was examined in normal muscle, tumor, and artery area simultaneously using MRI (SPGR to acquire 6 slices every 20 s). In parallel groups of animals injected with the nitroxides, tissue samples were taken over the same time period for image acquisition for ex vivo determination of total nitroxide concentration (oxidized plus reduced) by EPR spectroscopy. MRI assessed nitroxide reduction rates and total nitroxide present in the tissues are shown in Figure 7 and Table 1 for normal muscle, tumor, and blood. The two cell permeable nitroxides Tempol and 3CP exhibited distinct differences in the reduction rates of image intensity between normal and tumor tissue. In the case of Tempol, the decay rate in the tumor was ~ 3.5 times that observed in the normal tissue. For 3CP, the decay rate in the tumor was ~2 times higher than in normal leg. The total levels of Tempol and 3CP (nitroxide + hydroxylamine) as measured by EPR spectroscopy over the same time period in tumor and muscle homogenates was relatively constant suggesting that the decrease in nitroxide image intensity in MRI was a result of intracellular reduction of the nitroxide. In the case of the cell impermeable nitroxide 3CxP, no significant differences in MRI signal decay rates between tumor and muscle tissue were detected, and the MRI decay rates essentially paralleled the nitroxide tissue levels as examined by EPR. Similar findings were obtained in blood, suggesting that the reduction of Tempol and 3CP in the blood is a result global intracellular reduction and not clearance. 3CxP, since it is cell-impermable, was not reduced as evidenced by both MRI assessment and total nitroxide present in the blood. Nitroxide reduction rates for tissues just described and a few other tissues are shown in Table 1. These studies firmly establishes the use of cell-permeable nitroxides coupled with MRI to non-invasively examine differences in the redox status of tissues. While particular emphasis has been placed on differences in the

NIH-PA Author Manuscript

NIH-PA Author Manuscript

NIH-PA Author Manuscript

redox status in tumors compared with selected normal tissues, the technique possesses the potential to have broad applications to the study of other disease states, inflammatory processes, and other circumstances in which oxidative stress is implicated.

Assessment of Selective Radioprotection of Salivary Glands by Redox MRI

The ability to selectively protect normal tissues in cancer patients receiving radiation treatment would be most advantageous. If selective protection of normal tissues were possible, higher radiation doses could be delivered to the tumor accompanied with higher local control rates. The key, however, is selective normal tissue protection because if a systemic radioprotector also protects the tumor, no advantage would be realized. Amifostine, a FDA approved radioprotector for xerostomia (Koukourakis 2002; Scully et al 2006)remains controversial with respect to its ability to protect tumor as well as normal tissues (Yuhas 1983; Brizel & Overgaard 2003).

In vitro studies have clearly shown that nitroxide (oxidized form) is radioprotective; whereas, the hydroxylamine (reduced form) does not provide protection (Mitchell et al 1991; Krishna et al 1998; Mitchell et al 2003). Likewise, we have previously shown that Tempol protects against whole body radiation-induced lethality, with a dose-modifying factor of 1.4(Hahn et al 1992). Tempol when given at the same dose and timing (275 mg/kg, 10 min before radiation) as was used in whole body radiation study did not protect against local single radiation doses delivered to RIF tumors based on TCD_{50} comparisons(Hahn et al 1997). It was demonstrated in this study that Tempol was reduced to the non-radioprotective hydroxylamine faster in the tumor as opposed to bone marrow(Hahn et al 1992). Thus, at the time of radiation (10 min post-injection of Tempol), a higher concentration Tempol (radioprotective) was present in the normal tissue (bone marrow) than in the tumor when the Tempol levels were measured in the respective tissues ex vivo using EPR spectroscopy.

More recent studies have demonstrated that Tempol protects against radiation-induced salivary gland damage, but did not protect against radiation-induced tumor regrowth delay as shown in Figure 8 (Cotrim et al 2007). Five daily fractions of 6 Gy were delivered to only the animal's head. Tempol was injected IP, 275 mg/kg 10 min prior to each radiation fraction. As can be seen in Figure 8A, 5 × 6 Gy resulted in a reduction of saliva production ~54%. Five daily treatments of Tempol (i.p.) alone exhibited no toxicity and had no effect on salivary gland function (Fig. 8A); however, Tempol (i.p.) provided significant protection ($p < 0.001$) against radiation-induced salivary gland damage in replicate experiments. Figure 8B shows that administering Tempol at the same dose and timing as used in Figure 8A had no influence radiation-induced tumor regrowth delay. MR assessment of tissue levels of Tempol for each tissue (normal leg muscle, salivary gland region, and tumor) was also determined (Figure 9A). Transverse MR images were acquired to ensure that the target tissues were within the 2-mm slice selected for imaging (Fig. 9B). Dynamic T_1-weighted MR scans were then acquired before and after Tempol injection as shown in Figure 9C. The green areas show enhancement in MR intensity by Tempol, which quickly appeared at 30 s, peaked at ~1 min, and then gradually disappeared 8 min after injection. To establish the rate of disappearance (reduction) of Tempol in various tissues, selected ROI were outlined as shown in Figure 9D and MR intensity changes by Tempol in normal leg muscle, salivary gland region, and tumor were plotted as a function of time after injection as shown in Figure 10A. The decay in Tempol-mediated MR intensity was similar for normal leg muscle and the salivary gland region; however, the decay rate was significantly faster in the tumor region as shown in Figure 10B. These results suggest that Tempol provided salivary gland radioprotection and did not protect tumor, consistent with the hypothesis by the redox MRI results that differential radioprotection resides in faster reduction to the non-radioprotective hydroxylamine in tumor compared with normal tissues (Cotrim et al 2007).

NIH-PA Author Manuscript

NIH-PA Author Manuscript

NIH-PA Author Manuscript

This study provides the feasibility of evaluating Tempol as a radioprotector in clinical trials for patients with head/neck cancer being treated with radiation and utility of redox MRI. Coupling MRI with such a trial would permit a novel dimension that could provide extremely important information with respect to the timing of Tempol administration and radiation treatment. For example, before radiation treatment, a pilot Tempol/MRI study could be conducted to determine Tempol reduction rates of tumor and normal tissues encompassed in the proposed treatment field. Based on these reduction rates, the optimal timing of Tempol administration with respect to radiation treatment to provide selective radioprotection to normal tissues could be determined. The unique aspect of such an approach is made possible because the therapeutic agent in this case (Tempol) can be visualized by MRI. There are few therapeutic agents used in cancer management (excluding radiolabeled agents) that can be followed by noninvasive imaging. Before such an approach could be considered for clinical trials, more research will be required such as whether Tempol reduction rates in tissues change during fractionated radiation treatment.

Conclusions

Monitoring profiles of reduction/oxidation of nitroxide/hydroxylamines may actually serve as a viable approach to assess the global redox status in tissue using EPRI or MRI. The pharmacokinetics of the nitroxide can be obtained using either EPRI or MRI. Although EPRI can detect nitroxide free radicals directly and obtain images of nitroxide free radical distribution as well as redox maps, the poor image resolution and lack of anatomic detail limit its use in the clinical setting presently. On the other hand, the T_1-weighted MRI serves as an indirect detection modality of nitroxide contrast agents. The T_1-weighted spoiled gradient echo based dynamic MRI can give appropriate tumor redox status information with useful anatomic resolution. Functional nitroxide redox MRI could be used in the clinical setting to monitor redox changes in tumor and normal tissue in patients undergoing radiotherapy and other types of cancer treatment. Likewise, its potential applications in various disease states resulting from oxidative stress and inflammation remain to be explored.

Acknowledgments

This work was supported by the intramural research program of the Center for Cancer Research, National Cancer Institute, NIH.

References

Barbier EL, Lamalle L, Decorps M. Methodology of brain perfusion imaging. J Magn Reson Imaging 2001;13:496–520. [PubMed: 11276094]

Berliner JL, Fujii H. Magnetic resonance imaging of biological specimens by electron paramagnetic resonance of nitroxide spin labels. Science 1985;227:517–9. [PubMed: 2981437]

Berliner LJ, Fujii H, Wan XM, Lukiewicz SJ. Feasibility study of imaging a living murine tumor by electron paramagnetic resonance. Magn Reson Med 1987;4:380–4. [PubMed: 3035320]

Brasch RC. Work in progress: methods of contrast enhancement for NMR imaging and potential applications. A subject review. Radiology 1983;147:781–8. [PubMed: 6342034]

Brasch RC, London DA, Wesbey GE, Tozer TN, Nitecki DE, Williams RD, Doemeny J, Tuck LD, Lallemand DP. Work in progress: nuclear magnetic resonance study of a paramagnetic nitroxide contrast agent for enhancement of renal structures in experimental animals. Radiology 1983;147:773–9. [PubMed: 6844613]

Brizel DM, Overgaard J. Does amifostine have a role in chemoradiation treatment? Lancet Oncol 2003;4:378–81. [PubMed: 12788413]

Brown JM. SR 4233 (tirapazamine): a new anticancer drug exploiting hypoxia in solid tumours. Br J Cancer 1993;67:1163–70. [PubMed: 8512801]

NIH-PA Author Manuscript

NIH-PA Author Manuscript

NIH-PA Author Manuscript

Chen K, Glockner JF, Morse PD 2nd, Swartz HM. Effects of oxygen on the metabolism of nitroxide spin labels in cells. Biochemistry 1989;28:2496–501. [PubMed: 2543442]

Cotrim AP, Hyodo F, Matsumoto K, Sowers AL, Cook JA, Baum BJ, Krishna MC, Mitchell JB. Differential radiation protection of salivary glands versus tumor by Tempol with accompanying tissue assessment of Tempol by magnetic resonance imaging. Clin Cancer Res 2007;13:4928–33. [PubMed: 17699873]

DeGraff W, Hahn SM, Mitchell JB, Krishna MC. Free radical modes of cytotoxicity of adriamycin and streptonigrin. Biochem Pharmacol 1994;48:1427–35. [PubMed: 7945443]

Dunn JF, O'Hara JA, Zaim-Wadghiri Y, Lei H, Meyerand ME, Grinberg OY, Hou H, Hoopes PJ, Demidenko E, Swartz HM. Changes in oxygenation of intracranial tumors with carbogen: a BOLD MRI and EPR oximetry study. J Magn Reson Imaging 2002;16:511–21. [PubMed: 12412027]

Goldstein S, Samuni A, Hideg K, Merenyi G. Structure-activity relationship of cyclic nitroxides as SOD mimics and scavengers of nitrogen dioxide and carbonate radicals. J Phys Chem A 2006;110:3679–85. [PubMed: 16526651]

Greenlee RT, Hill-Harmon MB, Murray T, Thun M. Cancer statistics. CA Cancer J Clin 2001;51:15–36. [PubMed: 11577478]

Griffith OW. Mechanism of action, metabolism, and toxicity of buthionine sulfoximine and its higher homologs, potent inhibitors of glutathione synthesis. J Biol Chem 1982;257:13704–12. [PubMed: 6128339]

Hahn SM, Sullivan FJ, DeLuca AM, Krishna CM, Wersto N, Venzon D, Russo A, Mitchell JB. Evaluation of tempol radioprotection in a murine tumor model. Free Radic Biol Med 1997;22:1211–6. [PubMed: 9098095]

Hahn SM, Tochner Z, Krishna CM, Glass J, Wilson L, Samuni A, Sprague M, Venzon D, Glatstein E, Mitchell JB, et al. Tempol, a stable free radical, is a novel murine radiation protector. Cancer Res 1992;52:1750–3. [PubMed: 1551104]

Halliwell, B.; Gutteridge, JMC. Free Radicals in Biology and Medicine. Oxford University Press; London: 1999.

Herholz K, Coope D, Jackson A. Metabolic and molecular imaging in neuro-oncology. Lancet Neurol 2007;6:711–24. [PubMed: 17638612]

Hoh CK. Clinical use of FDG PET. Nucl Med Biol 2007;34:737–42. [PubMed: 17921026]

Huzjan R, Sala E, Hricak H. Magnetic resonance imaging and magnetic resonance spectroscopic imaging of prostate cancer. Nat Clin Pract Urol 2005;2:434–42. [PubMed: 16474681]

Hyodo F, Matsumoto K, Matsumoto A, Mitchell JB, Krishna MC. Probing the intracellular redox status of tumors with magnetic resonance imaging and redox-sensitive contrast agents. Cancer Res 2006;66:9921–8. [PubMed: 17047054]

Hyodo F, Murugesan R, Matsumoto KI, Hyodo E, Subramanian S, Mitchell JB, Krishna MC. Monitoring redox-sensitive paramagnetic contrast agent by EPRI, OMRI and MRI. J Magn Reson 2008;190:105–112. [PubMed: 18006345]

Keana JF, Pou S. Nitroxide-doped liposomes containing entrapped oxidant: an approach to the "reduction problem" of nitroxides as MRI contrast agents. Physiol Chem Phys Med NMR 1985;17:235–40. [PubMed: 3001795]

Keana JF, Pou S, Rosen GM. Nitroxides as potential contrast enhancing agents for MRI application: influence of structure on the rate of reduction by rat hepatocytes, whole liver homogenate, subcellular fractions, and ascorbate. Magn Reson Med 1987;5:525–36. [PubMed: 3437813]

Koo V, Hamilton PW, Williamson K. Non-invasive in vivo imaging in small animal research. Cell Oncol 2006;28:127–39. [PubMed: 16988468]

Koukourakis MI. Amifostine in clinical oncology: current use and future applications. Anticancer Drugs 2002;13:181–209. [PubMed: 11984063]

Krishna MC, Grahame DA, Samuni A, Mitchell JB, Russo A. Oxoammonium cation intermediate in the nitroxide-catalyzed dismutation of superoxide. Proc Natl Acad Sci U S A 1992;89:5537–41. [PubMed: 1319064]

Krishna MC, Russo A, Mitchell JB, Goldstein S, Dafni H, Samuni A. Do nitroxide antioxidants act as scavengers of O2-. or as SOD mimics? J Biol Chem 1996a;271:26026–31. [PubMed: 8824242]

NIH-PA Author Manuscript

NIH-PA Author Manuscript

NIH-PA Author Manuscript

Krishna MC, Samuni A, Taira J, Goldstein S, Mitchell JB, Russo A. Stimulation by nitroxides of catalase-like activity of hemeproteins. Kinetics and mechanism. J Biol Chem 1996b;271:26018–25. [PubMed: 8824241]

Krishna MC, DeGraff W, Hankovszky OH, Sar CP, Kalai T, Jeko J, Russo A, Mitchell JB, Hideg K. Studies of structure-activity relationship of nitroxide free radicals and their precursors as modifiers against oxidative damage. J Med Chem 1998;41:3477–92. [PubMed: 9719601]

Kuppusamy P, Chzhan M, Vij K, Shteynbuk M, Lefer DJ, Giannella E, Zweier JL. Three-dimensional spectral-spatial EPR imaging of free radicals in the heart: a technique for imaging tissue metabolism and oxygenation. Proc Natl Acad Sci U S A 1994;91:3388–92. [PubMed: 8159757]

Kuppusamy P, Afeworki M, Shankar RA, Coffin D, Krishna MC, Hahn SM, Mitchell JB, Zweier JL. In vivo electron paramagnetic resonance imaging of tumor heterogeneity and oxygenation in a murine model. Cancer Res 1998;58:1562–8. [PubMed: 9537265]

Kuppusamy P, Li H, Ilangovan G, Cardounel AJ, Zweier JL, Yamada K, Krishna MC, Mitchell JB. Noninvasive imaging of tumor redox status and its modification by tissue glutathione levels. Cancer Res 2002;62:307–12. [PubMed: 11782393]

Liu KJ, Bacic G, Hoopes PJ, Jiang J, Du H, Ou LC, Dunn JF, Swartz HM. Assessment of cerebral pO2 by EPR oximetry in rodents: effects of anesthesia, ischemia, and breathing gas. Brain Res 1995;685:91–8. [PubMed: 7583257]

Margolis DJ, Hoffman JM, Herfkens RJ, Jeffrey RB, Quon A, Gambhir SS. Molecular imaging techniques in body imaging. Radiology 2007;245:333–56. [PubMed: 17940297]

Matsumoto K, Narazaki M, Ikehira H, Anzai K, Ikota N. Comparisons of EPR imaging and T1-weighted MRI for efficient imaging of nitroxyl contrast agents. J Magn Reson 2007;187:155–62. [PubMed: 17433743]

Matsumoto K, Hyodo F, Matsumoto A, Koretsky AP, Sowers AL, Mitchell JB, Krishna MC. High-resolution mapping of tumor redox status by magnetic resonance imaging using nitroxides as redox-sensitive contrast agents. Clin Cancer Res 2006;12:2455–62. [PubMed: 16638852]

Mitchell JB, Russo A. The role of glutathione in radiation and drug induced cytotoxicity. Br J Cancer Suppl 1987;8:96–104. [PubMed: 3307879]

Mitchell JB, Russo A, Kuppusamy P, Krishna MC. Radiation, radicals, and images. Ann N Y Acad Sci 2000;899:28–43. [PubMed: 10863527]

Mitchell JB, Xavier S, DeLuca AM, Sowers AL, Cook JA, Krishna MC, Hahn SM, Russo A. A low molecular weight antioxidant decreases weight and lowers tumor incidence. Free Radic Biol Med 2003;34:93–102. [PubMed: 12498984]

Mitchell JB, DeGraff W, Kaufman D, Krishna MC, Samuni A, Finkelstein E, Ahn MS, Hahn SM, Gamson J, Russo A. Inhibition of oxygen-dependent radiation-induced damage by the nitroxide superoxide dismutase mimic, tempol. Arch Biochem Biophys 1991;289:62–70. [PubMed: 1654848]

Provenzale JM, Mukundan S, Barboriak DP. Diffusion-weighted and perfusion MR imaging for brain tumor characterization and assessment of treatment response. Radiology 2006;239:632–49. [PubMed: 16714455]

Samuni A, Krishna CM, Mitchell JB, Collins CR, Russo A. Superoxide reaction with nitroxides. Free Radic Res Commun 1990;9:241–9. [PubMed: 2167262]

Samuni Y, Gamson J, Samuni A, Yamada K, Russo A, Krishna MC, Mitchell JB. Factors influencing nitroxide reduction and cytotoxicity in vitro. Antioxid Redox Signal 2004;6:587–95. [PubMed: 15130285]

Schafer FQ, Buettner GR. Redox environment of the cell as viewed through the redox state of the glutathione disulfide/glutathione couple. Free Radic Biol Med 2001;30:1191–212. [PubMed: 11368918]

Scully C, Sonis S, Diz PD. Oral mucositis. Oral Dis 2006;12:229–41. [PubMed: 16700732]

Shapiro EM, Skrtic S, Sharer K, Hill JM, Dunbar CE, Koretsky AP. MRI detection of single particles for cellular imaging. Proc Natl Acad Sci U S A 2004;101:10901–6. [PubMed: 15256592]

Silva AC, Kim SG, Garwood M. Imaging blood flow in brain tumors using arterial spin labeling. Magn Reson Med 2000;44:169–73. [PubMed: 10918313]

Soule BP, Hyodo F, Matsumoto K, Simone NL, Cook JA, Krishna MC, Mitchell JB. The chemistry and biology of nitroxide compounds. Free Radic Biol Med 2007;42:1632–50. [PubMed: 17462532]

NIH-PA Author Manuscript

NIH-PA Author Manuscript

NIH-PA Author Manuscript

Stratford IJ, Adams GE, Bremner JC, Cole S, Edwards HS, Robertson N, Wood PJ. Manipulation and exploitation of the tumour environment for therapeutic benefit. Int J Radiat Biol 1994;65:85–94. [PubMed: 7905915]

Subramanian S, Matsumoto K, Mitchell JB, Krishna MC. Radio frequency continuous-wave and time-domain EPR imaging and Overhauser-enhanced magnetic resonance imaging of small animals: instrumental developments and comparison of relative merits for functional imaging. NMR Biomed 2004;17:263–94. [PubMed: 15366027]

Swartz HM. Principles of the metabolism of nitroxides and their implications for spin trapping. Free Radic Res Commun 1990;9:399–405. [PubMed: 2167277]

Swartz HM, Sentjurc M, Morse PD 2nd. Cellular metabolism of water-soluble nitroxides: effect on rate of reduction of cell/nitroxide ratio, oxygen concentrations and permeability of nitroxides. Biochim Biophys Acta 1986a;888:82–90. [PubMed: 3741890]

Swartz HM, Chen K, Pals M, Sentjurc M, Morse PD 2nd. Hypoxia-sensitive NMR contrast agents. Magn Reson Med 1986b;3:169–74. [PubMed: 3959885]

Torigian DA, Huang SS, Houseni M, Alavi A. Functional imaging of cancer with emphasis on molecular techniques. CA Cancer J Clin 2007;57:206–24. [PubMed: 17626118]

Utsumi H, Yamada K. In vivo electron spin resonance-computed tomography/nitroxyl probe technique for non-invasive analysis of oxidative injuries. Arch Biochem Biophys 2003;416:1–8. [PubMed: 12859975]

Yamada KI, Kuppusamy P, English S, Yoo J, Irie A, Subramanian S, Mitchell JB, Krishna MC. Feasibility and assessment of non-invasive in vivo redox status using electron paramagnetic resonance imaging. Acta Radiol 2002;43:433–40. [PubMed: 12225490]

Yu NY, Brown JM. Depletion of glutathione in vivo as a method of improving the therapeutic ratio of misonidazole and SR 2508. Int J Radiat Oncol Biol Phys 1984;10:1265–9. [PubMed: 6236185]

Yuhas JM. Efficacy testing of WR-2721 in Great Britain everything is black and white at the gray lab. Int J Radiat Oncol Biol Phys 1983;9:595–8. [PubMed: 6303993]

NIH-PA Author Manuscript

NIH-PA Author Manuscript

NIH-PA Author Manuscript

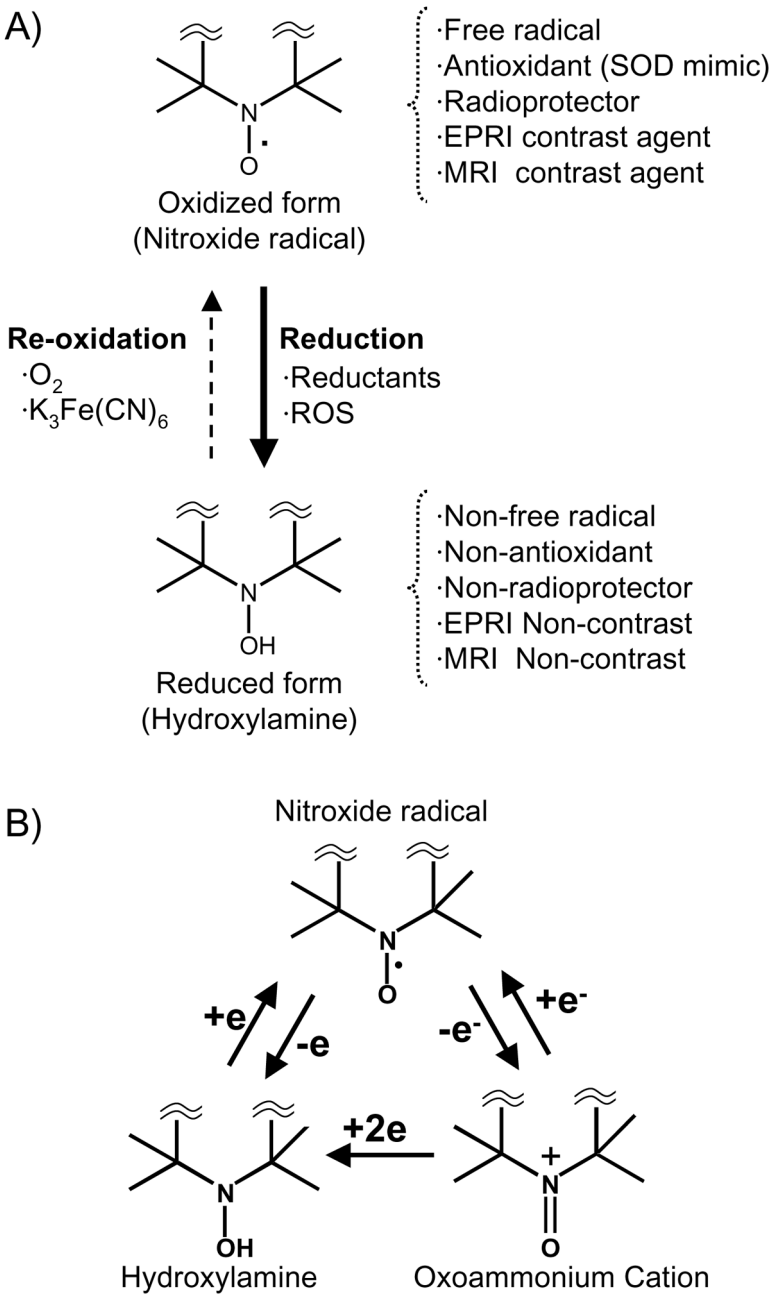

Figure 1.

A) Reversible one-electron reduction/oxidation showing the inter-conversion between the oxidized nitroxide (EPRI and MRI Contrast) and the corresponding reduced hydroxylamine (EPRI and MRI Non-contrast). B) Conversion of nitroxide radical to hydroxylamine or oxoammonium cation in vivo. Nitroxide compounds are found in vivo in an equilibrium between the nitroxide radical form which is detected by EPR, and the reduced form, known as the hydroxylamine, which is not detected. This equilibrium is dependent on the oxygen status and redox-status of the tissue milieu. Cellular redox processes convert the compound between the two states, thus the ratio of the two states is determined by the redox activity within the cell.

NIH-PA Author Manuscript

NIH-PA Author Manuscript

NIH-PA Author Manuscript

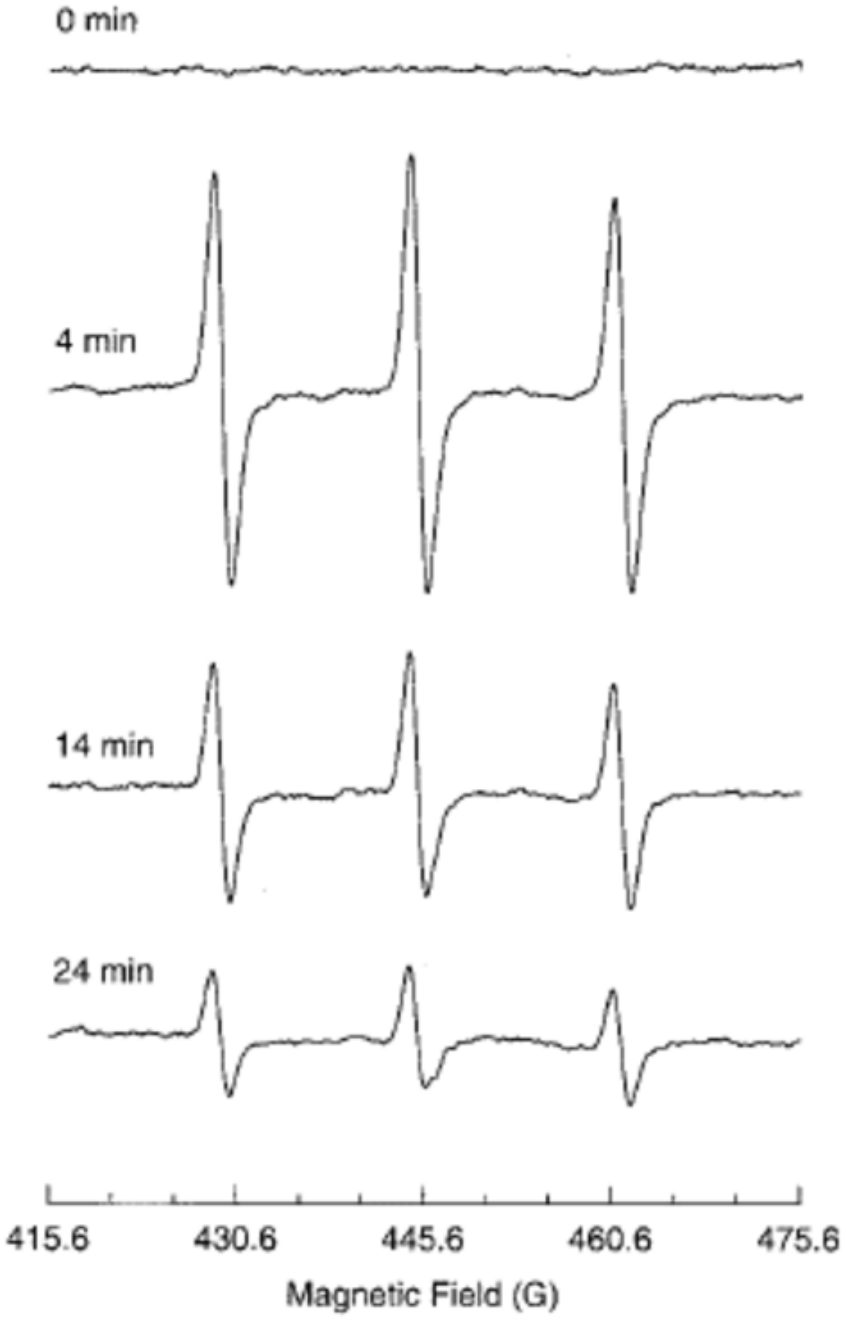

Figure 2.

EPR spectra of 3-CP nitroxide in a RIF-1 tumor. A tumor-bearing mouse under anesthesia was infused (i.v.) with a saline solution of 3-CP (185 mg/kg). The uptake and removal of the nitroxide in the tumor tissue was continuously measured *in vivo* using L-band (1.3 GHz) EPR spectrometer. The triplet signal attributable to 3-CP peaked at ~ 4 min and decayed gradually with a half-life of ~10 min. The triplet, arising because of hyperfine splitting from the 14N nucleus, is characterized with coupling constants 15.78 G and 16.30 G and peak-to-peak width 1.50 G. Measurement parameters: microwave power 8 mW; modulation amplitude, 1.0 G; modulation frequency, 100 kHz; scan time, 15 s. (Adapted with permission from reference Kuppusamy et al 2002)

NIH-PA Author Manuscript

NIH-PA Author Manuscript

NIH-PA Author Manuscript

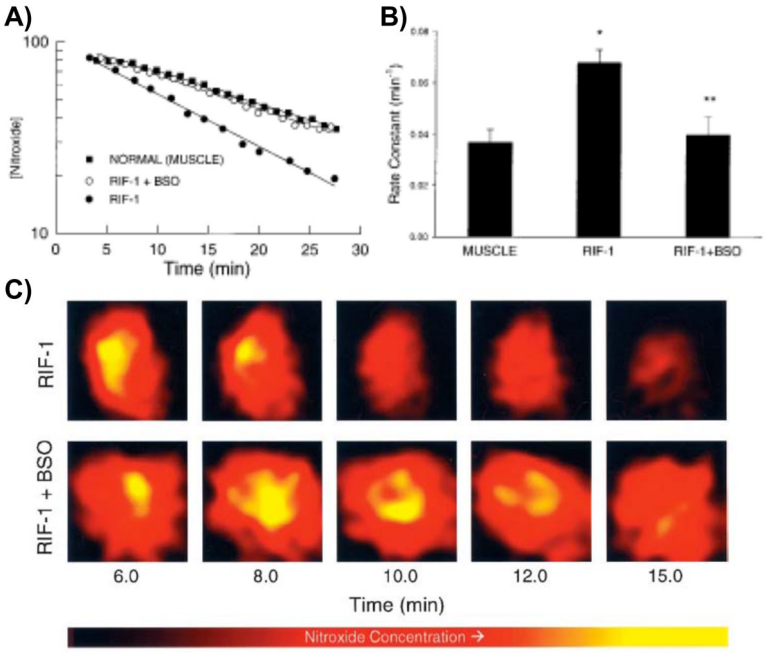

Figure 3.

Pharmacokinetics of nitroxide in normal muscle and tumor tissues. Time course of the EPR signal intensity of 3-CP in the normal leg muscle and tumor tissue of RIF-1 tumor-bearing mice, infused (i.v.) with a saline solution of 3-CP, were obtained by double integration of the spectra. A) The semilog plot shows the clearance of the nitroxide (in arbitrary units) as a function of time in the normal muscle and tumor tissue of untreated tumor-bearing mice and in the tumor tissue of mice treated (i.p.) with BSO (2.25 mmol/kg) 6 h before the measurements. The solid lines through the data points are linear fit to the respective data set, which suggests compliance with a pseudo first-order rate law. B) Bar-graph showing the measured pseudo first-order rate constants of nitroxide reduction in the tissues. The data represent mean ± SE of measurements on three to five mice per group. The rate constants were: untreated normal muscle, $0.037 \pm 0.005\ min^{-1}$; untreated tumor, $0.063 \pm 0.008\ min^{-1}$, and BSO-treated tumor, $0.052 \pm 0.006\ min^{-1}$. *, significantly different from normal muscle; **, significantly different from untreated RIF-1 tissue. C) Spatially resolved clearance of nitroxide in RIF-1 tumor tissue. After tail vein infusion of 3-CP, a series of two-dimensional images of the nitroxide from tumor (untreated and BSO-treated) were measured using L-band EPRI method. A few selected images and the corresponding approximate time after infusion are shown. The images represent the mean nitroxide concentration in a two-dimensional projection of the tissue volume ($10 \times 10\ mm^2$; depth, 5 mm) averaged over 1.5–2.0 min. The image data were acquired using a magnetic field gradient of 15 G/cm at 16 orientations in the two-dimensional plane. Each image within a series was normalized with respect to the maximum intensity in that series. The nitroxide in the tumor of BSO-treated mouse persisted longer, compared with that in the untreated mouse. (Adapted with permission from reference Kuppusamy et al 2002)

NIH-PA Author Manuscript

NIH-PA Author Manuscript

NIH-PA Author Manuscript

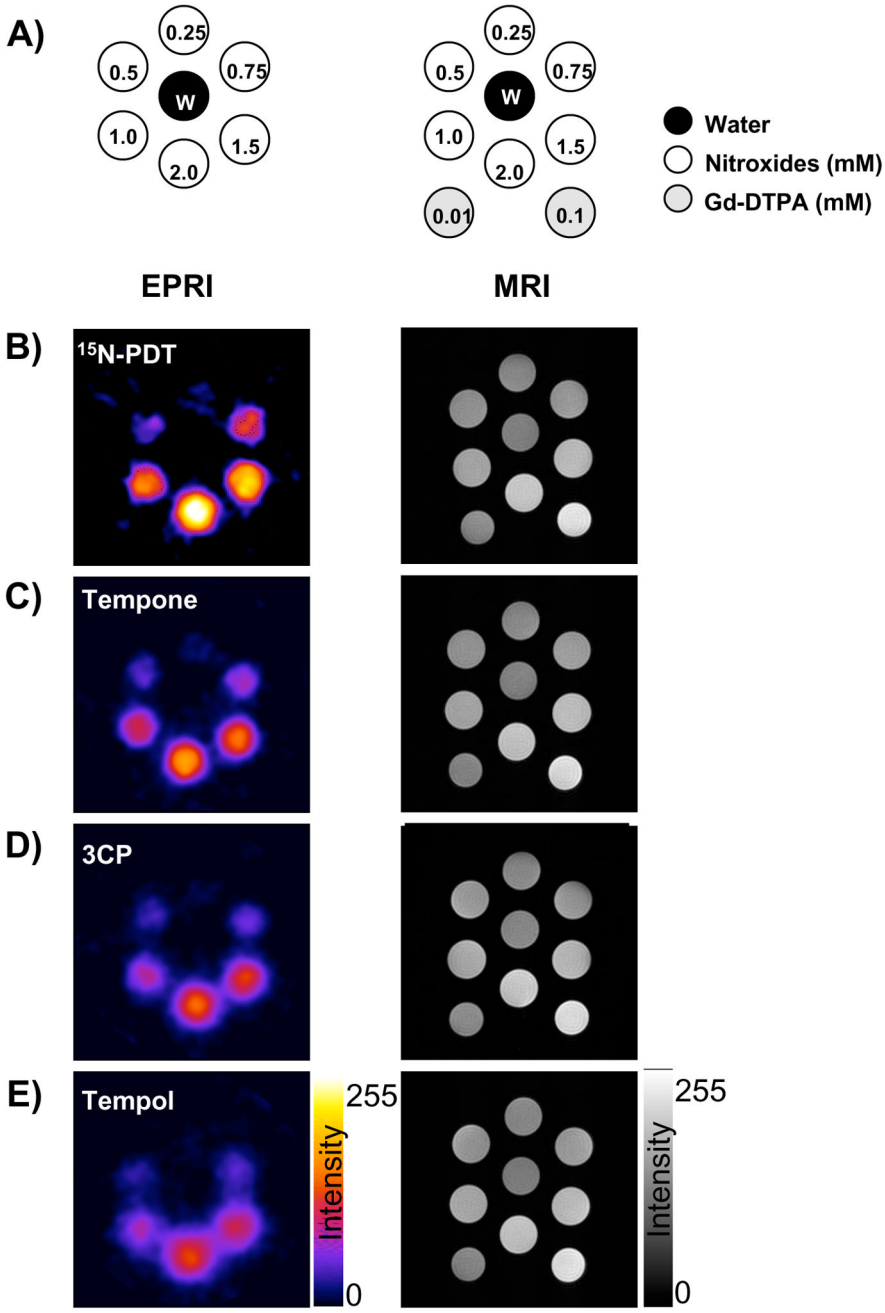

Figure 4.

The phantom images of four nitroxides obtained by EPRI and MRI. A) Schematics of the phantom. Additionally two tubes of 0.01 and 0.1 mM Gd-DTPA solution were added during MRI measurement. The EPRI (Left column) and MR (right column) intensity images of B) ^{15}N-PDT, C) Tempone, D) 3CP, E) Tempol were described. EPRI conditions were follows; 18 projections were obtained every 1 min. FOV was 3.2 × 3.2 cm. Microwave frequency was 300 MHz, microwave power 2.5 mW, field modulation frequency was 13.5 kHz, time constant 0.01 s, gradient was 4.7 G/cm, sweep width was 50 Gauss. MRI: SPGE sequence (TR = 75 ms, TE = 3 ms, Flip angle = 45°, NEX = 2) was employed to observe T_1 effect. Pixel resolution

was 256 × 256. FOV was 3.2 × 3.2 cm. All measurements were performed at room temperature (25 ± 2 °C). (Adapted with permission from reference Hyodo et al 2008)

NIH-PA Author Manuscript
NIH-PA Author Manuscript
NIH-PA Author Manuscript

NIH-PA Author Manuscript

NIH-PA Author Manuscript

NIH-PA Author Manuscript

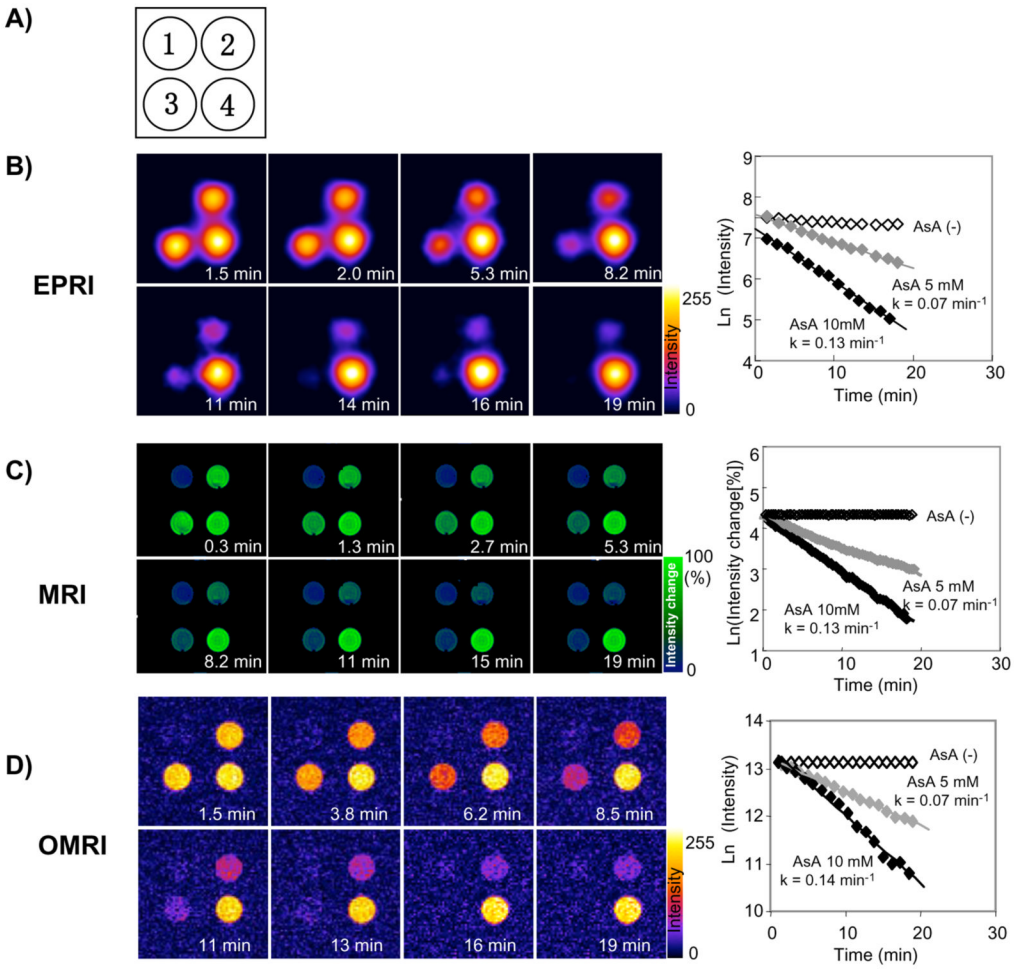

Figure 5.

Comparison of image intensity decay among three modalities. A) Schematic of the phantoms: Tube 1, PBS; Tube 2, 2 mM 3CP and 5 mM AsA; Tube 3, 2 mM 3CP and 10 mM AsA; Tube 4, 2 mM 3CP. Time course images and decay slops of B) EPRI, C) MRI, D) Overhauser MRI (OMRI) were obtained. After addition of AsA/PBS solution, the EPRI or OMRI measurements were started immediately and continuously measured up to 20 min. In the case of MRI, AsA/PBS was added using PE-10 tube 2 min after scanning was started. Therefore, time zero in the MRI experiment represents the time at addition of AsA solution. The experiments were repeated three or four times using with freshly prepared solutions. Semi-logarithmic plots of the time course of MRI signal change in the region of interest (ROI: 10 ×10 pixels) were used for decay rate calculation using imageJ software. Decay rate constants were obtained from the slope of linear portion of the decay curves. (Adapted with permission from reference Hyodo et al 2008)

NIH-PA Author Manuscript
NIH-PA Author Manuscript
NIH-PA Author Manuscript

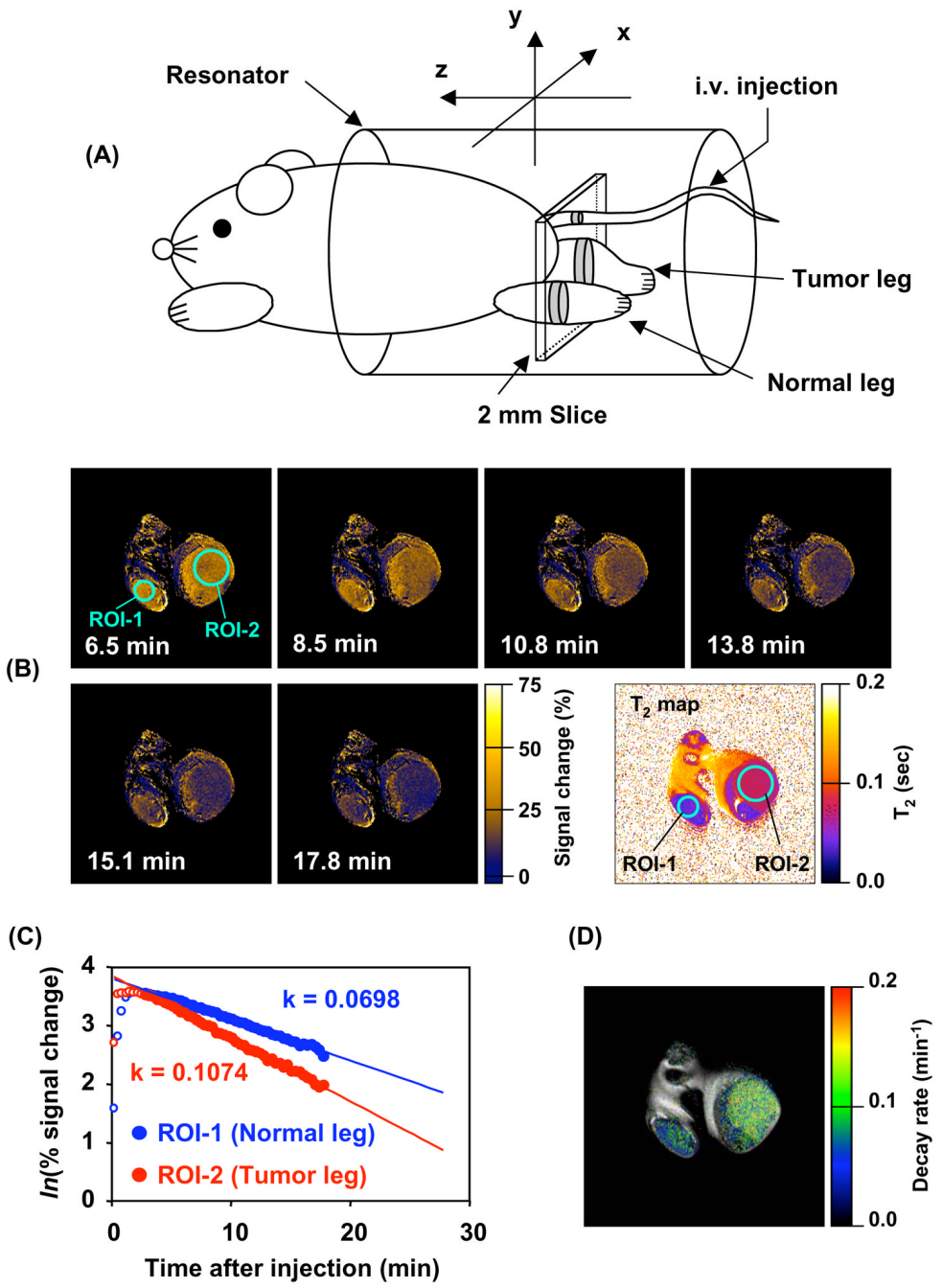

Figure 6.

(A) Experimental arrangement of the mouse in the MRI resonator and the slice selected to monitor the nitroxide levels used to examine the differences in nitroxide metabolism in tumor and normal tissue. (B) Sequence of T_1-weighted MR images as a function of time after intravenous administration of 3CP. Signal intensity in normal (ROI-1) and tumor leg (ROI-2) increased after 3CP administration and reached a maximum at 8.5 min. The nitroxide signal decreased thereafter faster in tumor region (ROI-1) than in normal tissue (ROI-2). (C) The rate of intensity change in each pixel was computed for each ROI and plotted as a function of time. The rate of intensity change in the normal leg was observed to be ~60% compared to that in tumor. (D) Parametric image redisplayed shows that tumor reduction globally is elevated

compared to the normal tissue. (Adapted with permission from reference (Matsumoto et al 2006))

NIH-PA Author Manuscript
NIH-PA Author Manuscript
NIH-PA Author Manuscript

NIH-PA Author Manuscript

NIH-PA Author Manuscript

NIH-PA Author Manuscript

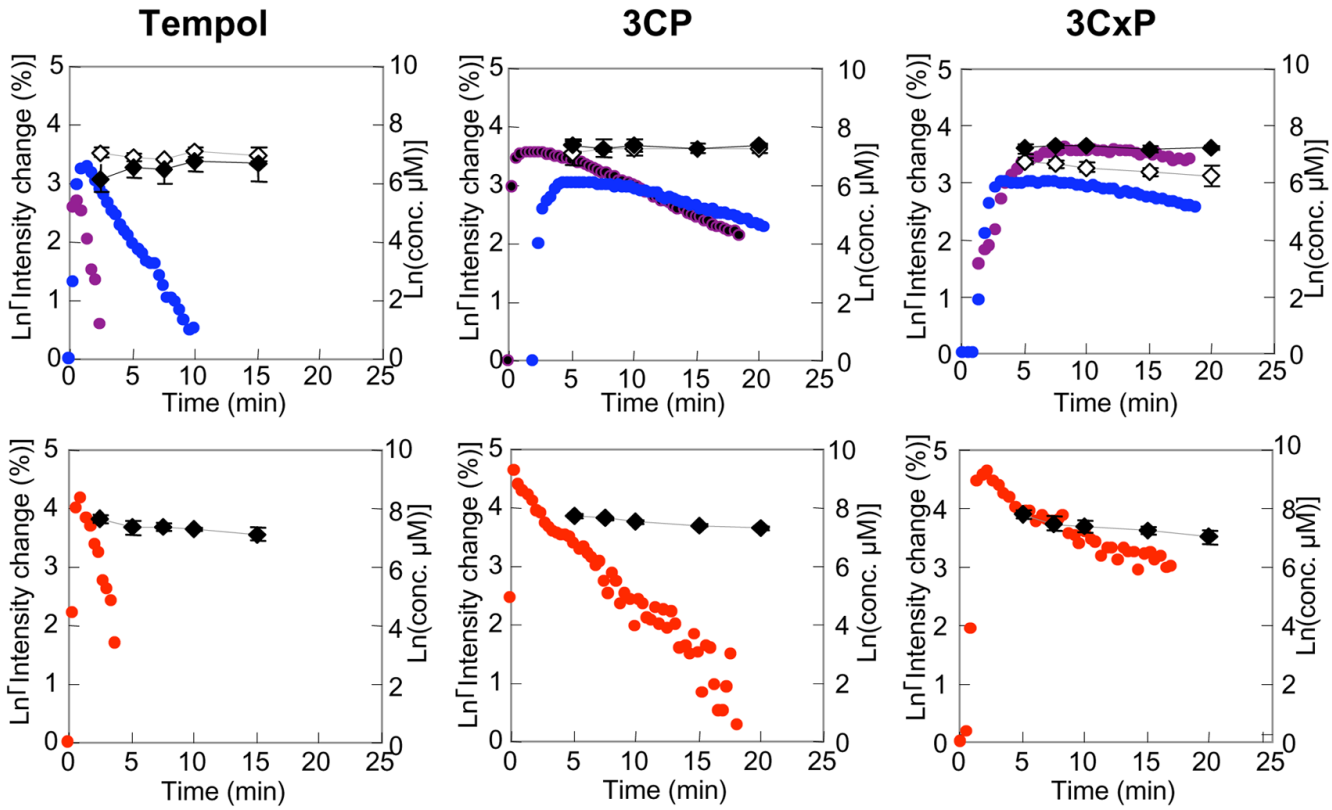

Figure 7.

The pharmacokinetics of oxidized form and total (oxidized and reduced form) nitroxide contrast agents in normal leg muscle, tumor, and blood. The pharmacokinetics of oxidized form of (A) Tempol, (B) 3CP, (C) 3CxP in normal tissue (blue), tumor tissue (purple), and artery (red) were obtained by SPGR MRI. The total nitroxide contrast agent concentration of (A) Tempol, (B) 3CP, (C) 3CxP in normal tissue (upper figure, gray), tumor tissue (upper figure, black) and blood (lower figure. black) were measured ex vivo by x-band EPR spectroscopy using 10 mM ferricyanide/PBS solution (final concentration was 2 mM). (Adapted with permission from (Hyodo et al 2006))

NIH-PA Author Manuscript

NIH-PA Author Manuscript

NIH-PA Author Manuscript

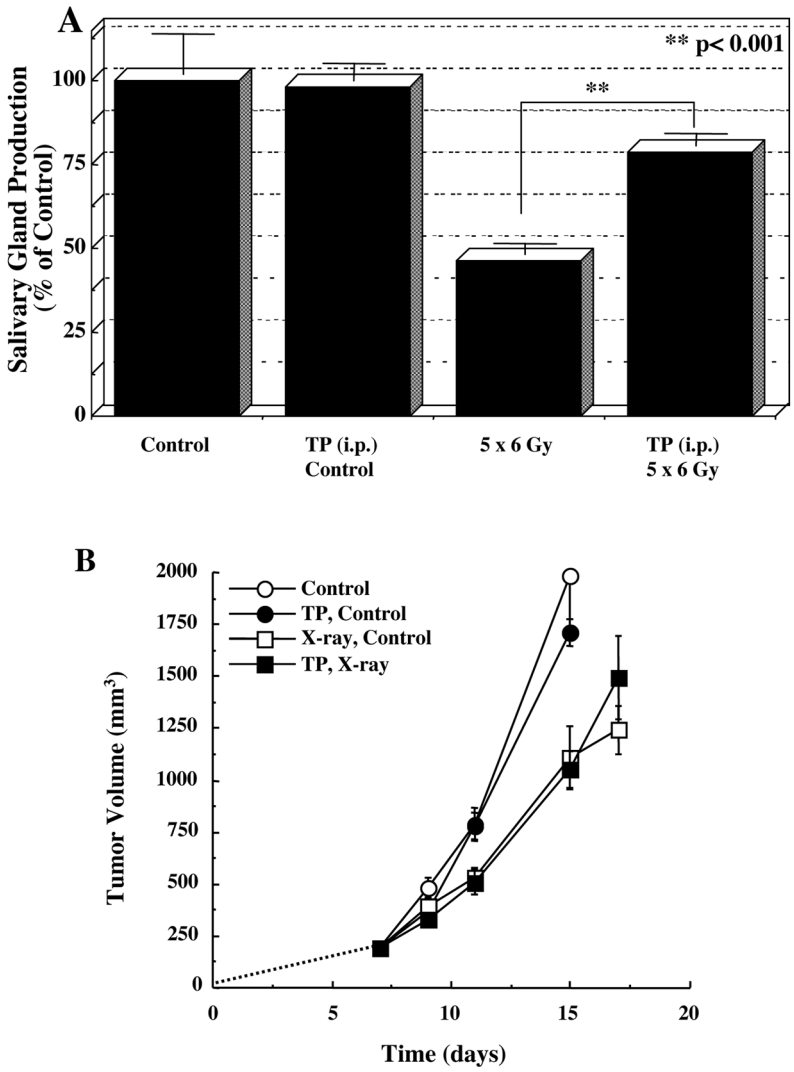

Figure 8.

A) Salivary gland production for fractionated radiation treatment with and without Tempol administration. B) Radiation tumor (SCCVII) regrowth study for local fractionated radiation treatment with and without Tempol administration. Tumors received 5 daily fractions (Monday-Friday) of 3 Gy (SCC VII) or 2 Gy (HT-29). Arrows on each plot indicate the days when radiation treatment was administered. (Adapted with permission from (Cotrim et al 2007))

NIH-PA Author Manuscript

NIH-PA Author Manuscript

NIH-PA Author Manuscript

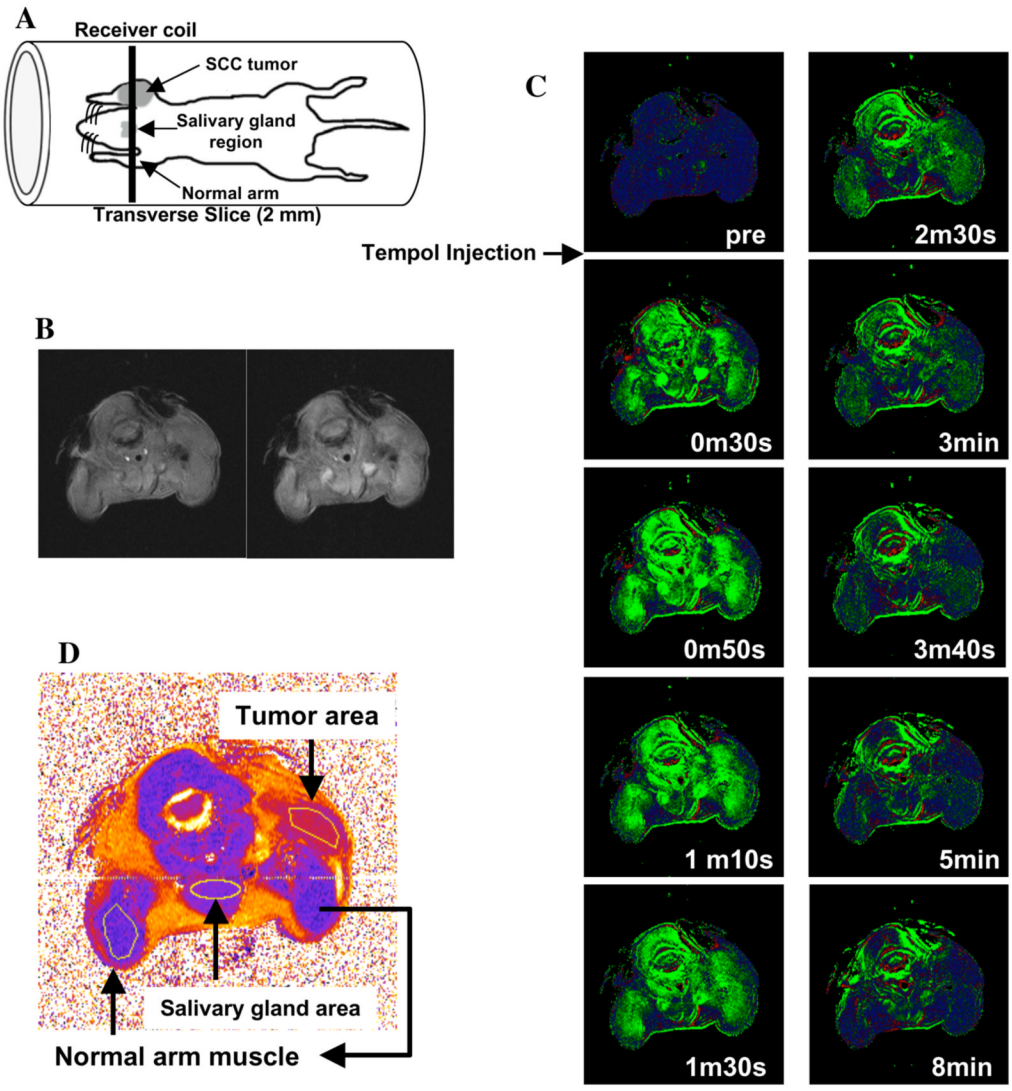

Figure 9.

A) Schematic of the placement of the mouse in the resonator and the slice selected for MRI experiments. A transverse slice (2 mm) covering the normal muscle tissue (Greenlee et al), salivary gland, and the tumor in the contra lateral leg was chosen to monitor nitroxide levels as a function of time. B) T_2-weighted images of adjacent slices before injecting Tempol to ensure that the target tissues were in the field of view. C) T1 weighted images of the selected region before injection of Tempol and as a function of time after i.v. Tempol injection. D) T_2 map of the slice and the regions of interest chosen in the normal leg, salivary gland, and tumor to monitor Tempol decay rates. (Adapted with permission from (Cotrim et al 2007))

NIH-PA Author Manuscript
NIH-PA Author Manuscript
NIH-PA Author Manuscript

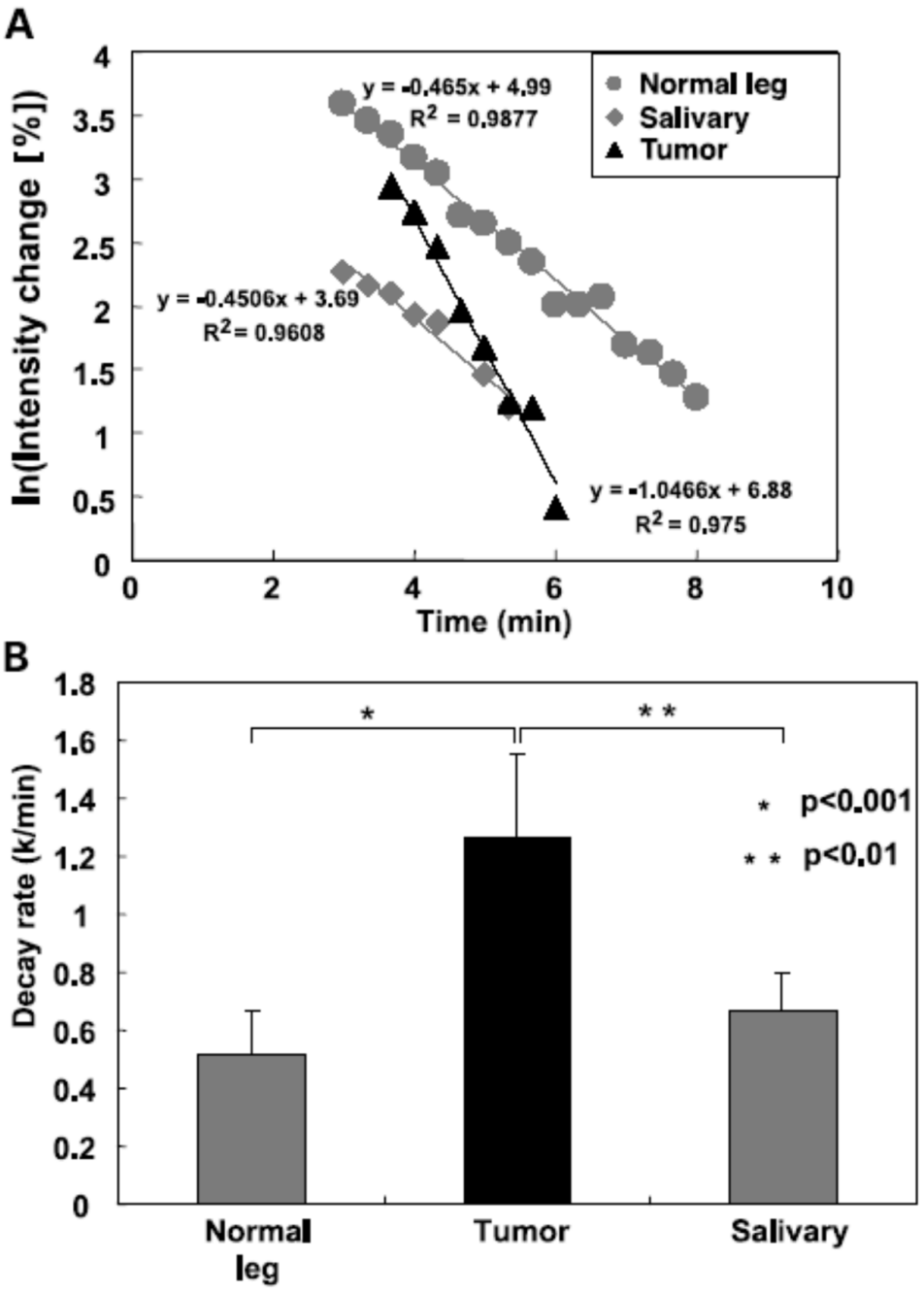

Figure 10.

A) Representative Tempol decay rates after i.v. injection in a mouse for the selected regions of interest shown in Figure 5D. B) Summary of decay rates from the three regions of interest in normal muscle, salivary gland, and tumor. (Adapted with permission from (Cotrim et al 2007))

NIH-PA Author Manuscript

NIH-PA Author Manuscript

NIH-PA Author Manuscript

Table 1

Decay Rate of Nitroxide Contrast Agents in Various Tissues

	Decay rate (min^{-1})		
Tissue	**Tempol**	**3CP**	**3CxP**
Normal leg	0.32 ± 0.03	0.056 ± 0.013	0.029 ± 0.014
Tumor leg	1.1 ± 0.2 **	0.107 ± 0.020 *	0.020 ± 0.014
Blood	1.0 ± 0.2	0.364 ± 0.008	0.4 ± 0.2
Left kidney	1.5 ± 0.2	0.30 ± 0.05	0.046 ± 0.006
Right kidney	1.2 ± 0.3	0.29 ± 0.04	0.050 ± 0.005
Salivary gland	0.79 ± 0.3	ND	ND

Values are indicated as means ± SD. The three mice after each nitroxide (total 9 mice) injection were measured and obtained serial images (total 360 images) of six slices of each mouse during 20 min. * and ** indicate significant differences between the muscle and tumor with * $p < 0.05$, ** $p < 0.01$. T_1-weighted images (6 slices and 60 continuous imaging: total 360 images) were acquired during 20 minutes, using SPGR. A solution of nitroxide contrast agents in PBS (1.5 μmol/g b.w.) was injected via tail vein cannulation, 2.0 min after starting scan. The conditions of MRI were follows; TR = 75 ms, TE = 3 ms, FA = 45°, N_{EX} = 2, Scan time 20 s. Image resolution = 256 × 256, FOV was 3.2 × 3.2 cm, slice thickness was 2.0 mm. Number of slices was 2. (Adapted with permission from: (Hyodo et al 2006; Cotrim et al 2007)